Relative Dominance of Physical versus Chemical Effects on the Transport of Adhesion-Deficient Bacteria in Intact Cores from South Oyster, Virginia

ARTICLE *in* ENVIRONMENTAL SCIENCE AND TECHNOLOGY · APRIL 2002

Impact Factor: 5.33 · DOI: 10.1021/es010144t · Source: PubMed

8 AUTHORS, INCLUDING:

Hailiang Dong
Miami University
185 PUBLICATIONS **3,566** CITATIONS
SEE PROFILE

Mary F Deflaun
Geosyntec Consultants Inc
69 PUBLICATIONS **2,273** CITATIONS
SEE PROFILE

Mark Fuller
CB&I Federal Services
66 PUBLICATIONS **1,292** CITATIONS
SEE PROFILE

Timothy D Scheibe
Pacific Northwest National Laboratory
135 PUBLICATIONS **1,984** CITATIONS
SEE PROFILE

Environ. Sci. Technol. **2002**, *36,* 891−900

Relative Dominance of Physical versus Chemical Effects on the Transport of Adhesion-Deficient Bacteria in Intact Cores from South Oyster, Virginia

HAILIANG DONG,*,† T. C. ONSTOTT,† MARY F. DEFLAUN,‡ MARK E. FULLER,‡ TIMOTHY D. SCHEIBE,§ SHERYL H. STREGER,‡ RANDI K. ROTHMEL,‡ AND BRIAN J. MAILLOUX†

Department of Geosciences, Princeton University, Princeton, New Jersey 08544, Envirogen, Inc., Princeton Research Center, 4100 Quakerbridge Road, Lawrenceville, New Jersey 08648, and Pacific Northwest National Laboratory, P.O. Box 999, MSIN K9-36, Richland, Washington 99352

Bacterial transport experiments were conducted using intact sediment cores collected from sites on the Delmarva Peninsula near South Oyster, VA, to delineate the relative importance of physical and chemical heterogeneity in controlling transport of an adhesion-deficient bacterial strain. Electron microscopy revealed that the sediments consisted of quartz and feldspar with a variable amount of clay and iron and aluminum hydroxide coatings on the grains. A nonmotile, Gram-negative indigenous groundwater strain, designated as *Comamonas* sp. DA001, was injected into the cores along with a conservative tracer bromide (Br). DA001 cells were $1.2 \times 0.6\ \mu$m in size with a hydrophilic surface and a slightly negative surface charge. Bacterial breakthrough preceded that of Br. This differential advection phenomenon can be accounted for by reduction of the effective porosity for the bacteria relative to Br. The distribution of cells remaining in the core as determined by scintillation counting and phosphor imaging techniques was variable, ranging from nearly uniform concentrations throughout the core to exponentially decreasing concentrations with distance from the point of injection. The fraction of bacterial retention in the core was positively correlated with the abundance of the metal hydroxides and negatively correlated with grain size. Because grain size was inversely correlated with the abundance of the metal hydroxide coatings, it was necessary to separate the effects of grain size and mineralogy. The fraction of the bacterial retention accounting for the effect of grain size, the collision efficiency, exhibited no correlation with the abundance of the metal hydroxides, indicating that the bacterial retention was primarily controlled by grain size. Reasons for the lack of influence of mineralogy on bacterial transport include (i) the slightly negatively charged bacterial surfaces; (ii) an insufficient heterogeneity of sediment surface properties; and (iii) the masking of the positive charge of the metal hydroxide surfaces by adsorbed organic carbon (up to 1180 ppm). This study demonstrates that the laboratory-based bacterial transport experiments are effective in delineating physical versus chemical controlling factors and provide an important link to field-based bacterial transport studies.

Introduction

Bacterial transport in porous media is of increasing importance in developing technologies to bioremediate contaminated aquifers (*1*, *2*), in preventing facilitated transport of pollutants by bacteria (*3*), in improving the recovery of oil from the subsurface (*4*), and in assessing the movement of pathogens or genetically engineered microorganisms (*5*, *6*). Bioremediation via bioaugmentation, i.e., the injection of degradative bacteria into a contaminated aquifer, has become a cost-effective way to remediate groundwater contaminated with chlorinated solvents (*2*) and may prove essential for the remediation of heavy metals and radionuclides (*7*, *8*).

One vital requirement for successful bioagumentation is the delivery of the injected bacteria to the zones of contamination. Bacterial adsorption to mineral grain surfaces, which is controlled by biological, physical, and chemical factors, significantly impairs dispersion of bacteria during bacterial transport experiments (*9*−*11*). The extended Derjaguin−Landau−Verwey−Overbeek (DLVO) theory describes the total interaction force between bacterial and mineral grain surfaces as the sum of the double layer, London−van der Waals, and acid−base type potential energies over the distance separating the surfaces (*12*). If the total interaction force is attractive, the injected bacteria are more likely to attach to mineral surfaces than when the force is repulsive. It has been demonstrated that the presence of iron and aluminum hydroxides retards bacterial transport due to the electrostatic attraction between negatively charged bacteria and the positively charged hydroxides at subneutral groundwater pH (*13*). The adsorption of organic matter onto the iron and aluminum hydroxide surfaces reduces the attraction by masking their positive charges. Whereas the theoretical calculations of the DLVO interaction forces are relatively straightforward, validation using representative experimental systems is needed.

Well-controlled bacterial transport studies have been conducted in columns filled with either glass beads or homogenized sediments. Because the homogenization and repacking process destroys the natural structure of physical and chemical heterogeneity, results from the repacked cores may not accurately represent transport behavior of bacteria in the subsurface (*14*) and are difficult to extrapolate to field studies. This study addresses the relative importance of physical and chemical factors on the transport of one bacterial strain in a number of intact sediment cores. Such cores are often the only means of assessing rates and distances of bacterial transport prior to injection in the field, so understanding core-scale processes and their relationship to field-scale transport is an essential step in prediction of field-scale transport.

A single bacterial strain was selected to maximize breakthrough in the field. Once a bacterial strain is chosen for injection, it is important to understand the limiting conditions

* Corresponding author present address: Department of Geology, Miami University, Oxford, OH 45056; telephone: (513)529-2517; fax: (513)529-1542; e-mail: dongh@muohio.edu.
† Princeton University.
‡ Envirogen, Inc.
§ Pacific Northwest National Laboratory.

10.1021/es010144t CCC: $22.00
Published on Web 01/19/2002

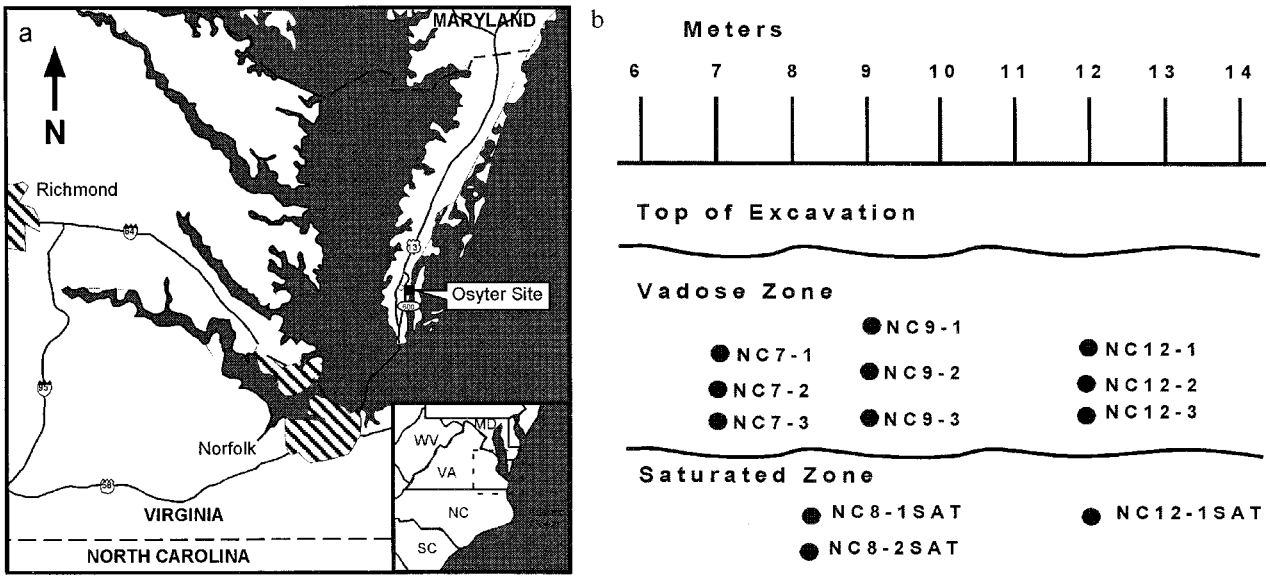

FIGURE 1. (a) Location map of the Oyster Site in the Delmarva Peninsula of Virginia. (b) Excavation cross section layout map showing intact core locations.

of bacterial transport, particularly if transport distance is to be increased via alterations of physical and chemical properties of a groundwater aquifer. Although the choice of an adhesion-deficient strain provides a good model for addressing physical control on bacterial transport, it may not be ideal to examine the chemical effect. Nonetheless, the selected strain is negatively charged and exhibits heterogeneity from one population to another. These cell properties allow us to evaluate the effect of the chemical heterogeneity.

Materials and Methods

Field Site and Intact Core Collection. The South Oyster site is located on the southern Delmarva Peninsula situated on the eastern coast of Virginia between the Chesapeake Bay and the Atlantic Ocean (Figure 1). The sediments at the site consist of unconsolidated to weakly cemented, well-sorted, medium- to fine-grained, late Pleistocene sands, and pebbly sands of the Wachapreague formation. The Narrow Channel (NC) focus area has been extensively characterized using geophysical and hydrological methods (*15*). Intact cores were collected from above and below the water table from an excavation at the NC site (Figure 1). Intact cores were collected in aluminum tubes of 7.5 cm in diameter × 50 cm in length. To collect intact cores from vadose zone, the tubes were driven into a pit face parallel to the regional groundwater flow direction. Saturated intact cores were collected from below water table (by 0.5 m) by trenching down with a backhoe and quickly extracting cores before the trench collapsed. Because of the unconsolidated nature of sediment from the saturated zone, it was possible to disturb the pore structure of cores during the collection process. However, any deformation feature was not visible once the cores were split. Fine details, such as iron oxide bands, were clearly preserved, suggesting minimal disturbance. Thus, the term "intact core" is still used in this paper. The cores were identified with the prefix NC combined with the horizontal location and the depth. Cores collected from below water table were appended with the suffix "SAT". The four intact cores used in this study were NC12-1SAT, NC12-3, NC8-1SAT, and NC8-2SAT.

Groundwater Geochemistry. Field measurements of groundwater geochemistry indicated that NC groundwater was aerobic (5−7 mg/L of dissolved oxygen), was slightly acidic (pH 5.5−6), contained <1 mg/L of dissolved organic carbon, and had an ionic strength of 0.003 M. Ambient groundwater temperature was 15 °C. Bacterial transport experiments were performed using natural groundwater. However, artificial groundwater (*16*), made based on the chemistry of the natural NC groundwater but without colloidal materials and dissolved organic matter, was used for cell culturing and radiolabeling.

Bacterial Strain Isolation and Characterization. The indigenous strain, *Comamonas* sp. DA001, was isolated from NC groundwater, and an adhesion-deficient variant was selected (*17*). The electrophoretic mobility of bacterial cells in NC natural groundwater was determined using a mobility analyzer (*18*). Multiple samples from the same culture as well as from multiple cultures were used to assess intra- and inter-population heterogeneity. Cell size and morphology were characterized by transmission electron microscopy (*19*). Typically, 40−50 measurements were made. Cell hydrophobicity (10−20 measurements per culture) was determined by measuring the contact angle between a bacterial lawn and a drop of NC natural groundwater (*18*).

Bacterial Strain Culturing and Radiolabeling. DA001 cells were grown on sodium acetate in basal salts medium with 1.35 μCi/mL of ^{35}S-labeled methionine added for radiolabeling (*17*), followed by wash and starvation in NC artificial groundwater for 72 h at 15 °C. Conversion of radioactivity (dpm) to concentration (cells/mL or g) is described elsewhere (*17*). Correction for ^{35}S decay was applied to data based on the time between the start of the experiment and the time of sample analyses. The average percent adhesion was determined prior to injection using a standardized assay (*21*) with NC natural groundwater and homogenized NC site sediment. The percent adhesion of the cells injected into cores NC12-1SAT and NC12-3 was 27%, whereas that of the cells injected into cores NC8-1SAT and NC8-2SAT was 46%.

Injection and Effluent Sampling. Details concerning the experimental setup are described elsewhere (*16*, *17*). Initial injections of 0.5 core pore volume of bromide (Br) in NC groundwater were performed. Starved cells were washed, suspended in 0.5 pore volume of NC groundwater to the desired cell concentrations (see Table 1), and injected into the cores in a 15 °C environmental chamber. The wide range of the cell injection concentration was selected to evaluate its effect on transport. The similarity in the transport behavior of the bacteria among the four cores (see below) suggested that any filtering or other cell−cell interaction resulting from

TABLE 1. Experimental Configuration for the Four Cores Used in This Study

parameter	NC12-1SAT	NC12-3	NC8-1SAT	NC8-2SAT
core length (m)	0.5	0.5	0.4	0.4
nominal pore volume (mL)	865	678	520	528
bromide pulse length (h)	4.70	3.50	5.50	3.53
bromide concentration (mg/L)	50.0	50.0	50.9	45.3
bromide flow rate (mL/h)	92.02	96.86	47.27	74.72
DA001 pulse length (h)	4.70	3.50	4.70	3.07
DA001 influent concentration (cells/mL)	3.15×10^7	3.89×10^7	1.22×10^{10}	1.14×10^9
DA001 flow rate (mL/h)	101.35	86.40	53.26	84.82
total cells injected	1.5×10^{10}	1.18×10^{10}	3.05×10^{12}	2.96×10^{11}
initial total dpm injected	1.77×10^8	1.39×10^8	1.10×10^9	1.07×10^8
CFU/dpm	85	85	2770	2770
total time of DA001 experiment (h)	252	252	216	216

high influent cell concentration for NC8-1SAT and NC8-2SAT was not significant. Once introduction of cells was complete, NC groundwater was continuously pumped through the cores. The pH of the cell suspension and eluted fractions shifted from ~6 to 7.2 over the experimental duration. Effluent fractions were collected at 20-min intervals (~17 mL per fraction). The radioactivity (dpm/mL) of one aliquot (0.5 mL) was measured with a scintillation counter (*20*). Multiple measurements of the same sample gave rise to an analytical error of ~5%. When the radioactivity in the fractions fell to a background level (~50 dpm/mL), the transport experiment was terminated.

Quantification of Attached Bacterial Concentration in Sediment. To correlate the retained cell concentration to the physical and chemical heterogeneity, the aluminum casing of the cores was cut, and the cores were split longitudinally. The concentration of the retained bacteria was determined in both core halves using the sediment subsampling (*17*) and the phosphor imaging techniques (*22*). The sediment subsampling method directly measures radioactivity (hence bacterial concentration). The phosphor imaging method offers a high-resolution visualization of bacterial retention (spatial resolution of 88 μm).

For subsampling, a core half was divided into a grid of 28 rows longitudinally and 5 columns laterally (*17*). The sediment from each grid volume was homogenized, and the radioactivity was measured with a scintillation counter (*20*). Multiple measurements of the same sample gave rise to ~5% error. The phosphor imaging technique was employed to directly image the distribution of radioactivity (and therefore bacteria) in the sediment. Six epoxy-fixed thin sections (5 × 7.5 cm, lateral × longitudinal distance) were made from one core half, exposed to a tritium imaging screen, and the recorded radioactivity was read by a Molecular Dynamics Imager (Molecular Dynamics, Sunnyvale, CA) (*22*). The resulting images were digitized at a spatial resolution of 5 × 4 mm (lateral × longitudinal distance) to obtain radioactivity. This resolution resulted in a grid of approximately 9 × 19 digitized rectangles per regular thin section. The digitized radioactivity was linearly proportional to bacterial concentration and was converted to it (*22*). Multiple analyses of the same sample resulted in an analytical error of 2−3%.

Electron Microscopic Characterization of Sediments. To correlate the retained bacterial concentration (from phosphor image digitization) with the physical and chemical heterogeneities of the cores, it was necessary to determine the physical and chemical parameters of the sediment. The thin sections, from which the phosphor images were taken, were analyzed for the areal abundance of iron and aluminum hydroxides, grain size, and porosity for all 5 × 4 rectangles using a scanning electron microscope (SEM) (*22*) Each rectangle contained 700−800 grains, and the arithmetic number average of all grain sizes in each rectangle was recorded and used in regression analyses.

SEM image analysis could only measure pore size greater than ~10 μm, measure grain size greater than ~10 μm, and was not capable of distinguishing fine-grained clays from the iron and aluminum hydroxides, both of which were present as grain coatings of quartz and feldspars. Because clays and the metal hydroxides are of opposite charge at subneutral pH (*23*), their distinction is important. Transmission electron microscopy and chemical extraction (see below) were used to determine the relative proportions of clays and the metal hydroxides in the sediment. The results showed that the grain coatings of NC12-1SAT were dominated by the metal hydroxides with <10% clays; therefore, it was not necessary to separate clays and the metal hydroxides. The grain coatings of NC8-1SAT were dominated with clays (90%) with some metal hydroxides (10%). Therefore, the areal abundance of the grain coatings measured by SEM in each rectangle was multiplied by a factor of 0.1 to obtain the areal abundance of the metal hydroxides. The other two cores were handled in a similar fashion.

Fe/Al and Organic Carbon Extraction. An additional means to quantify the amount of the metal hydroxides was by the citrate−bicarbonate−dithionite extraction (*24*). Twelve samples were selected from the sediment subsamples of NC8-1SAT and were split into two aliquots. One aliquot was used for the extraction of Fe and Al, and the other was used for extraction of adsorbed organic carbon. Dissolution of chlorite (identified by electron microscopy) during the extraction of Fe and Al was corrected based on measured Si concentration. The extraction results of Fe and Al standards, goethite and gibbsite, indicated that the method extracted all Fe from iron hydroxide, but Al extraction was not complete. Therefore, Al concentrations were likely underestimated. Twelve 1-g sediment subsamples from NC8-1SAT were treated with 0.1 N NaOH to extract adsorbed organic carbon. The concentration of organic carbon was determined by the combustion method following the U.S. EPA Protocol 9060/415.1 using a Dohrmann DC-190 carbon analyzer (Tekmar Dohrmann, Santa Clara, CA). Measured organic carbon concentration was corrected for biomass assuming 10^{-13} g of carbon per bacterium.

ζ-Potential Measurement of Sediment. The ζ-potential is an important parameter for characterizing the electrostatic interaction between bacterial and sediment surfaces. It was desirable to measure ζ-potential from each 5 × 4 mm rectangle. Unfortunately, ζ-potential measurements using streaming potential techniques require several grams of sediment, and it was not possible for each rectangle. The ζ-potentials of only several subsamples from NC8-1SAT, before and after organic carbon extraction, were measured in NC groundwater (*18*). These measurements were not significant for statistical analysis, and the areal abundance of the metal hydroxides measured by SEM was used for multiple regression analysis.

Multiple Regression. After collection of the above data, multiple regression analysis was then performed between the bacterial retention and the sediment physical (grain size) and chemical (the abundance of the metal hydroxides) properties. Because each 5 × 4 rectangle had a different

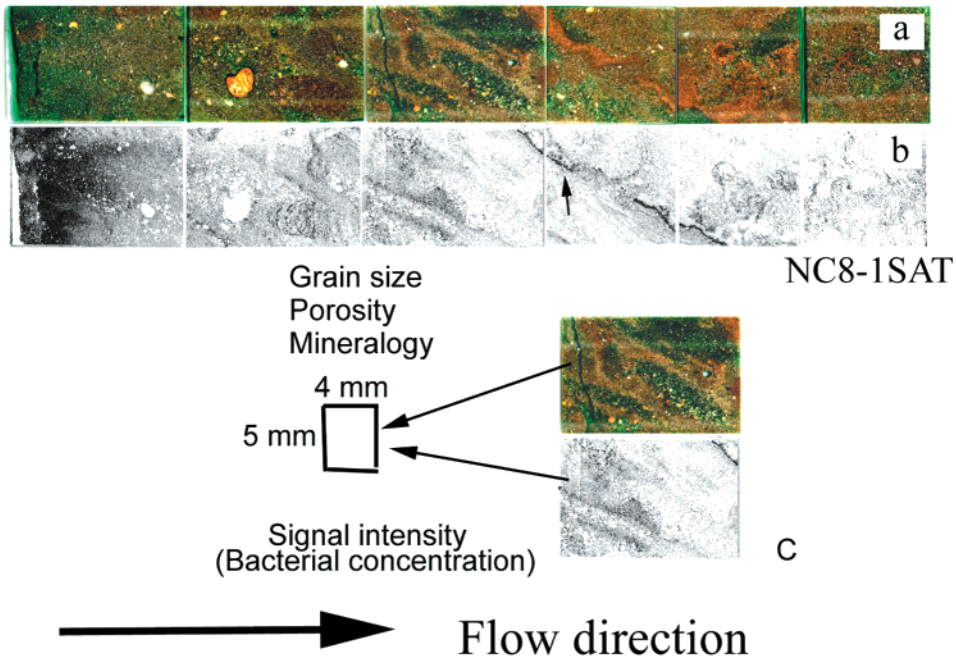

FIGURE 2. (a) Intact core (NC8-1SAT) constructed from six thin sections showing bands cross-cutting the flow. (b) Corresponding phosphor image showing the distribution of the retained bacteria in the core. (c) Schematic showing procedure of discretization of the physical (grain size and porosity) and chemical (abundance of the metal hydroxides) heterogeneity and concentration of retained bacteria in the core. The retained bacterial concentration can be correlated with grain size and the abundance of the metal hydroxides (see text for details). In section 4, a cross-cutting band is visible where DA001 cells are preferentially retained on one side facing the influent end (see arrow). In the middle of the band, a channel appears to be developing where the bacteria are forced to pass through.

incoming bacterial concentration, digitized bacterial concentration was normalized to result in the fraction of retention (R_i), the ratio of the number of bacteria retained in one rectangle to the total number of bacteria that entered the rectangle. Mathematically, the fraction of retention is defined as (*22*)

$$R_i = S_i/(C_0 - \sum S_{i-1}) \quad (1)$$

where R_i is the fraction of cell retention in rectangle i, C_0 is the initial bacterial concentration, S_i is the bacterial concentration in rectangle i, and $\sum S_{i-1}$ is the sum of all bacterial concentrations previous to rectangle i. Each core had approximately 9 grid columns of 5 mm in spacing and 114 grid rows of 4 mm in spacing. The bacteria, once they entered one grid column, were assumed not to leave this grid column, and other bacteria from adjacent grid columns were assumed not to join them either. This assumption was tested and proven to be valid.

Numerical Modeling. The factors controlling the transport of bacteria can be further investigated through numerical simulations to derive transport parameters. These parameters are useful when predictions for field-scale transport are made (*25*). All model results were obtained using the CXTFIT code (*26*) with the one-site nonequilibrium model option with no predation and growth terms. The parameter estimation capabilities of CXTFIT were first used to estimate advective velocity and dispersivity using the bromide breakthrough data. Given the known flow rate and the core volume, the effective porosity for bromide was then calculated. CXTFIT was again used to estimate four parameters (advective velocity, dispersivity, attachment rate coefficient, and detachment rate coefficient) from the observed breakthrough curves for DA001, and the effective porosity for DA001 and differential advection factors were calculated. Estimated pore velocity and dispersivity values for Br were used as initial inputs. Differential advection factor is defined as the ratio of the DA001 pore velocity to that of Br, modified to account for any differences in bulk flow rates between Br and bacterial experiments. Mathematically, it is defined as $(Q/Av)_{DA001}/(Q/Av)_{Br}$, where Q is the volumetric flow rate (mL/h), A the is core cross-section area (cm^2), and v is the pore velocity (m/d or cm/h). Forward simulations were then performed using the derived parameters to predict the profile of attached bacteria at 30 h and at the end of the experiment. Model parameters (representative of transport at the core scale) were then compared to those derived from direct measurements performed at subcore scales to provide independent assessment of parameters and to test the general appropriateness of the assumed model.

Results

Bacterial Properties. Bacterial strain DA001 was slightly negatively charged with the electrophoretic mobility of $-0.45 \pm 0.01 \times 10^{-8}$ m^2 V^{-1} s^{-1} for one batch of cells (27% percent adhesion, i.e., those injected into cores NC12-1SAT and NC12-3) and $-1.01 \pm 0.21 \times 10^{-8}$ m^2 V^{-1} s^{-1} for the other batch of cells (46% percent adhesion, i.e., those injected into cores NC8-1SAT and NC8-2SAT). Multiple samples from the same batch of culture did not show any variability. TEM micrographs showed that the strain was rod-shaped with a size of 1.2 ($\pm$ 0.1) $\times$ 0.6 ($\pm$ 0.1) μm. No flagella or surface polymers were observed. The contact angle measurement of 29.8 ± 0.9 indicated that it was hydrophilic.

Sediment Properties. The NC sediment was dominated by quartz, feldspar, clays, and aluminum and iron hydroxides. Cores NC12-1SAT and NC8-1SAT displayed cross-cutting bands in photos of the thin sections (Figure 2a). The SEM analyses revealed that the bands consisted of fine-grained quartz and feldspar (smaller than the surrounding areas by a factor of 2) with abundant clays and aluminum and iron hydroxides. The relationship between these bands and bacterial retention is shown in Figure 2b and discussed below. Rectangles for the SEM analyses were matched to those for digitization of the phosphor images (Figure 2c). Systematic SEM measurements resulted in approximately 1000 mea-

TABLE 2. Experimental Results and Inferred Parameters

parameter	NC12-1SAT	NC12-3	NC8-1SAT	NC8-2SAT
permeability (Darcy)	43.3	43.1	17.2	18.2
Measured Core Properties				
SEM measured porosity (%)	0.26 ± 0.03	0.35 ± 0.04	0.30 ± 0.04	0.34 ± 0.03
grain size (μm)	286 ± 41	293 ± 25	219 ± 47	210 ± 43
abundance of coatings (%)	2.81 ± 1.0	3.0 ± 0.5	4.4 ± 1.3	2.2 ± 1.2
metal hydroxide abundance (%)	2.81 ± 1.0	0.30 ± 0.04	0.44 ± 0.16	0.22 ± 0.12
DA001 effluent recovery (%)	67.2 ± 0.1	61.3 ± 0.1	57.7 ± 0.1	53.2 ± 0.2
DA001 retention[a] (%)	24.0 ± 0.2	21.2 ± 0.2	12.1 ± 0.0	8.8 ± 5.2
pore vol at which DA001 max C/C_0 reached	0.38	0.48	0.36	0.20
av local attachment rate (K_f, h^{-1}) (based on sorbed data)	0.06 ± 0.02	0.06 ± 0.02	0.10 ± 0.03	na[b]
Bromide CXTFIT Fitted Transport Parameters				
pore velocity (m/d)	1.22	1.27	0.76	0.85
dispersivity (m)	0.016	0.007	0.037	0.015
Br derived effective porosity	0.44	0.45	0.36	0.52
DA001 CXTFIT Fitted Transport Parameters				
pore velocity (m/d)	2.28	1.61	1.18	0.94
dispersivity (m)	0.021	0.008	0.025	0.016
DA001 effective porosity	0.26	0.32	0.27	0.53
differential advection factor	1.67	1.41	1.33	1.00
attachment rate (K_f, h^{-1})	0.20	0.08	0.09	0.11
detachment rate (K_r, h^{-1})	0.011	0.004	0.003	0.014

[a] Our previous study (*17*) indicated that poor mass balance was due to incomplete counting of radioactivity of sediment subsamples by scintillation counter, and grinding of sediments recovered all missing biomass. Therefore, all missing biomass in these cores was assumed in sediment, although not all sediment subsamples of these cores were ground. [b] na, not available.

surements of grain size, porosity, and areal abundance of the metal hydroxides for each core with average values shown in Table 2. Systematic trends were apparent in NC8-2SAT, where grain size and the metal hydroxide abundance remained constant from the influent end to the middle of the core, followed by a decrease in grain size and an increase in the metal hydroxide content toward the effluent end. Within each core, an inverse correlation was identified between the areal abundance of grain coatings (both clays and metal hydroxides) and grain size (Figure 3a), indicating that the fine-grained coatings were preferentially present on small grains of quartz and feldspars. Such a correlation was also observed between the areal abundance of the metal hydroxides and grain size (data not shown).

The extractable Fe and Al concentrations for the sediment of NC8-1SAT were in the range of 236−623 and 513−1305 mg/kg with means of 334 ± 119 and 702 ± 216 mg/kg, respectively. The sum of the extractable Fe and Al concentrations was comparable to that measured by the SEM analyses. The adsorbed organic carbon for the sediment subsamples of NC8-1SAT exhibited a large range from 84 to 1180 mg/kg and was inversely correlated with average grain size (Figure 3b). The ζ-potential for the NC8-1SAT sediment subsamples ranged from −10 to −1 mV with an average of −5.2 ± 1.8 mV. The majority of the subsamples possessed ζ-potentials from −3 to −6 mV. The ζ-potential was weakly correlated with the extractable Fe (Figure 3c) and became less negative (by 1−2 mV) after the adsorbed organic carbon was extracted.

Breakthrough and Effluent Recovery. The bacterial breakthrough curves had similar shapes for the four cores and were characterized by a sharp peak with no significant tailing (Figure 4). The maximum cell concentration (C/C_0) was reached at less than one pore volume with values of C/C_0 less than 0.5 for all four cores (Table 2). The effluent recovery ranged from 53% to 67% (Table 2). The breakthrough of bacteria preceded that of the Br tracer (Figure 4). This phenomenon is referred to here as differential advection and is discussed further below. For the cores collected from the saturated zone, the maximum C/C_0 was lower, and the breakthrough peak was wider. A small amount of tailing was observed in NC12-1SAT (Figure 4).

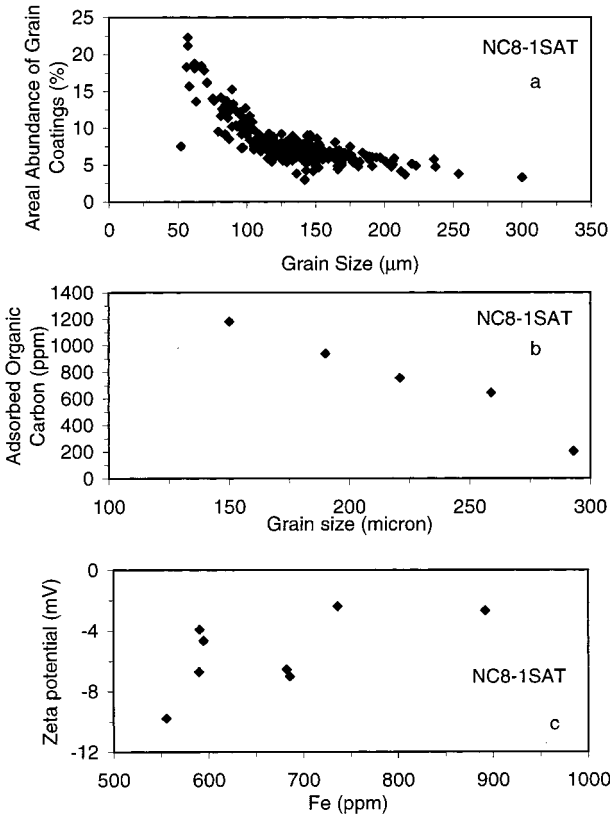

FIGURE 3. (a) Correlation between grain size and the areal abundance of the coating materials (both clay and hydroxide) for NC8-1SAT showing a negative correlation. (b) Correlation between the extractable organic matter and grain size. (c) Correlation between ζ-potential and extractable Fe for the sediment subsamples from core NC8-1SAT.

Bacterial Retention in Sediment. The profiles of adsorbed bacterial concentration determined by the subsampling method exhibited little variability for NC12-1SAT and NC12-3 in both lateral and longitudinal directions (Figure 5). For

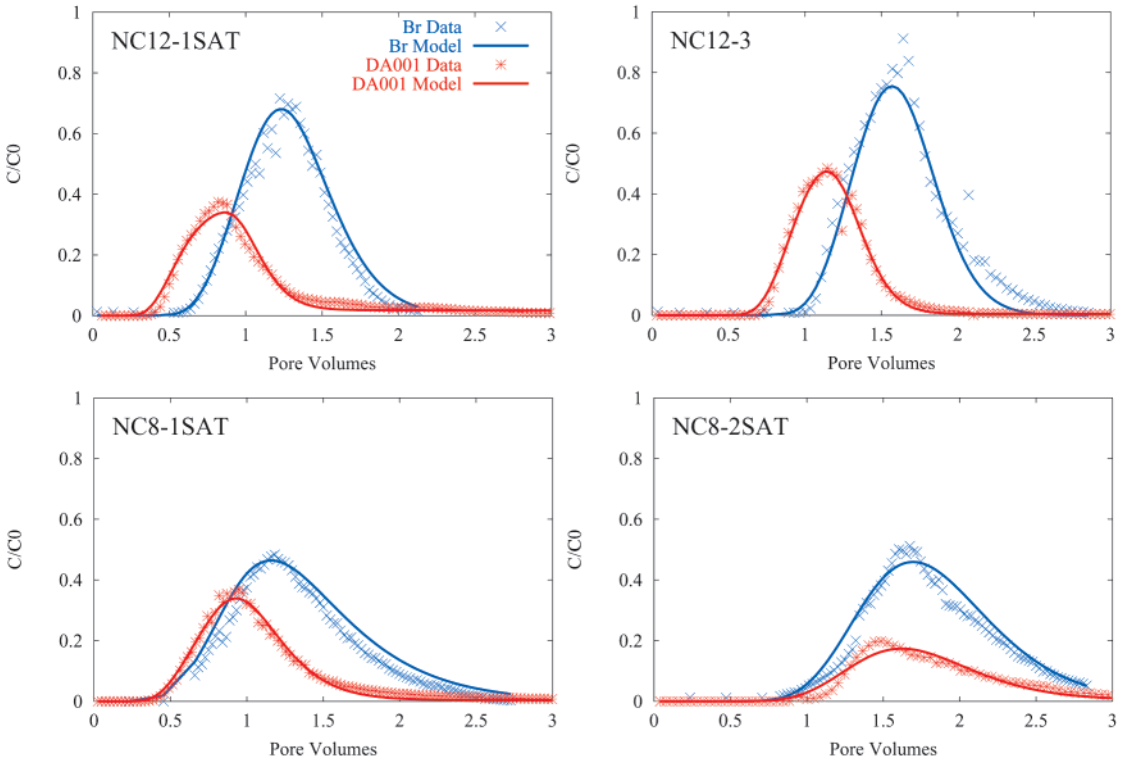

FIGURE 4. Observed and model breakthrough curves of DA001 and bromide in the four cores: (a) NC12-1SAT, (b) NC12-3, (c) NC8-1SAT, and (d) NC8-2SAT. The key in panel a applies to all four plots.

NC8-1SAT, the bacterial retention decreased longitudinally and decreased from the center to the edges in the lateral direction. The NC8-2SAT core showed a decrease in the cell retention with distance from the influent end up to 25 cm, followed by an increase to the effluent end with an asymmetrical distribution of cell retention laterally. Bacterial distribution determined by the phosphor imaging revealed more variability (Figure 2). The images of both NC12-1SAT and NC12-3 displayed a fairly uniform distribution of bacterial concentration in the longitudinal direction with enhancements along the fine-grained, metal hydroxide-rich bands (data not shown). The retained bacteria in NC8-1SAT were concentrated near the influent end and decreased exponentially toward the effluent end (Figure 2b). The bacterial concentration along the fine-grained, metal hydroxide-rich bands was much higher than that in band-free regions. The side of the band facing the influent end retained more bacteria than the side facing the effluent end.

Relationship between the Fraction of Bacterial Retention and the Physical and Chemical Heterogeneity. A multiregression analysis between R_i (dependent variable) and grain size (d_i) and the abundance of the metal hydroxides (independent variables) revealed that R_i was nearly equally controlled by these two parameters. However, grain size and abundance of the metal hydroxides was inversely correlated (Figure 3a); therefore, only one of these two variables was independent. To deconvolute these two parameters, it was necessary to transform the fraction of retention (R) to collision efficiency (α).

Filtration Theory and Calculation of Collision Efficiency. Clean-bed filtration models have previously been applied to quantify bacterial attachment to aquifer sediments (*27*). In this approach, attachment rate is represented as a function of porosity, grain size, and two filtration parameters: the collector efficiency (η) and the collision efficiency (α). Because the collision efficiency accounts for the effects of grain size and can be directly calculated, any correlation between the collision efficiency and the abundance of the metal hydroxides is indicative of the chemical effect. The collision efficiency was calculated for every 5 × 4 mm rectangle for which bacterial concentration, grain size, porosity, and areal abundance of the metal hydroxides were determined.

The procedure for calculating the collision efficiency is described previously (*22*). Briefly

$$\alpha_i = -\frac{2}{3}\frac{d_i}{(1-\theta_i)\eta_i L_i}\ln(1-R_i) \qquad (2)$$

$$k_f = \frac{3}{2}\frac{(1-\theta_i)\eta_i\alpha_i v_i}{d_i} = -\frac{\ln(1-R_i)v_i}{L_i} \qquad (3)$$

where R_i is the fraction of cell retention in rectangle i (calculated from eq 1), α_i is the collision efficiency, d_i is the grain size, θ_i is the porosity, η_i is the collector efficiency, L_i is the thickness of the rectangle parallel to flow (4 mm), v_i is the pore velocity, and k_f is the attachment rate coefficient. The calculation of α required two steps (*22*). The first step involved calculation of η based on grain size and porosity from SEM measurements of individual rectangles, bacterial length (1.2 μm), bacterial approach velocity (Table 2), bacterial density (1.075 g/mL), water density and viscosity at 15 °C, and Hamaker constant (4.1×10^{-21} J). Hamaker constant was calculated based on surface tension components of the bacteria and the NC sediment (*18*). The second step involved application of eq 2 once η was calculated. The calculation results indicated that α values varied from 0.003 to 0.025 with the majority of the values in the range of 0.005−0.015. No correlation was apparent between the collision efficiency and the metal hydroxide abundance for each of the four cores. The attachment rate coefficient (K_f) exhibited a broad range of values with a similar mean for all four cores (Table 2).

Modeling Results. The linear attachment and detachment kinetic model is able to reproduce the breakthrough curves during the main pulse of the breakthrough (first three pore

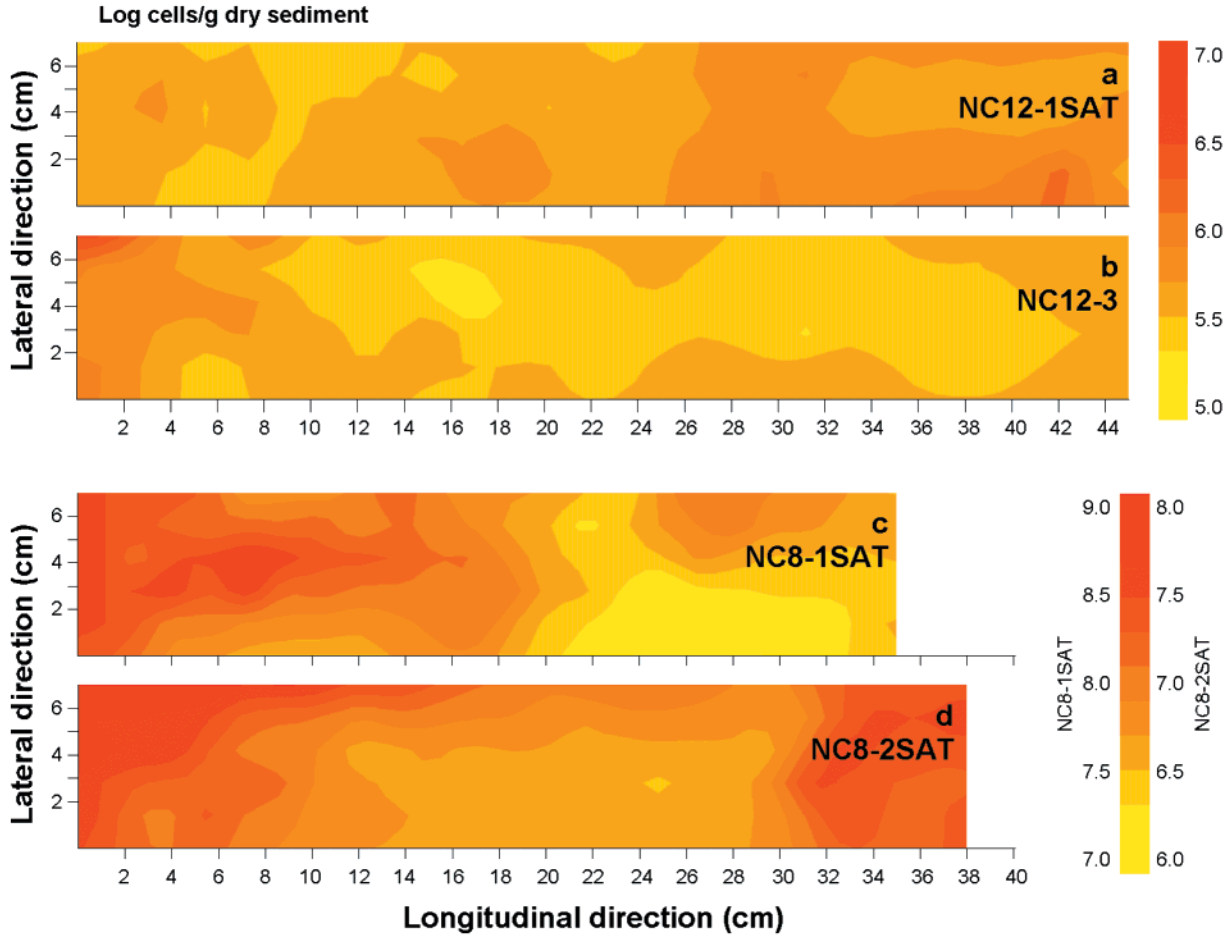

FIGURE 5. Contour plots of the distribution of the retained bacteria in the four cores as determined from the scintillation counting of subsamples. The legends show log cells/g of sediment in dry weight.

volumes, Figure 4). However, the model slightly overestimates effluent concentrations at longer times (i.e., breakthrough tailing). Observed profiles of attached bacteria along the core are fairly constant for NC12-1SAT and NC12-3, falling between the simulated profiles at time 30 h (slope downward from the influent end) and at the end of the experimental period (slope upward from the influent end) (Figure 6). Cores NC8-1SAT and NC8-2SAT both exhibit high concentrations of attached bacteria near the influent end relative to the model predictions, and NC8-2SAT also exhibits higher concentrations near the effluent end than the model prediction (Figure 6).

The pore velocity, dispersivity, and effective porosity for DA001 are significantly different from those for bromide (Table 2). Except for NC8-2SAT, the model derived porosity for DA001 is similar to the SEM measured porosity, suggesting that SEM only measured macropores experienced by DA001 cells. The calculated differential advection factor significantly varies from one core to another and is positively correlated with the abundance of grain coatings (both metal hydroxides and clays). The values of K_f derived from parameter estimation modeling at the full-core scale compare favorably to the mean of the values calculated on the subcore grid using eq 3 but tend to be somewhat higher, especially for those cores exhibiting a high degree of differential advection (i.e., a high metal hydroxide content) (Table 2).

Discussion

Experimental Reproducibility. Although it was desirable to evaluate experimental reproducibility, it was nearly impossible for several reasons. First, each individual core was different in physical and chemical characteristics, and there were no replicate intact cores. Second, post-injection core analysis was destructive, and it was not possible to inject additional bacteria into the same core. Even if a core could be preserved and re-injected with another pulse of bacteria, deposited bacteria from the previous experiment could affect the transport of subsequently injected bacteria. Nonetheless, a qualitative comparison between the similar cores (i.e., between NC8-1SAT and NC8-2SAT) with the same flow velocity and percent cell adhesion indicated that both breakthrough and sediment retention were fairly reproducible.

Differential Advection. Early breakthrough of microorganisms as compared to that of a conservative tracer has been observed in several studies (*28*−*30*), and the primary mechanisms include the following: (i) volume size exclusion (exclusion of bacteria from smaller pores due to their inability to fit into them); (ii) preferential flow path through high conductivity regions; and (iii) hydrodynamic retardation (or chromatography) (exclusion of bacteria from the lower velocity regions of a pore throat due to their size) (*31, 32*).

The positive correlation between the differential advection factor and the abundance of the grain coatings (Table 2) suggests that the fine-grained coatings are responsible for the reduced porosity (up to 18%) and therefore enhanced pore velocity for the bacteria relative to Br. Unlike the bacterial attachment process, the porosity reduction is merely a physical phenomenon, and all fine-grained coatings (including clays and metal hydroxides) should have the same effect reducing porosity. Therefore, it is the fine-grained nature of the coatings (not their positive or negative surfaces) that are

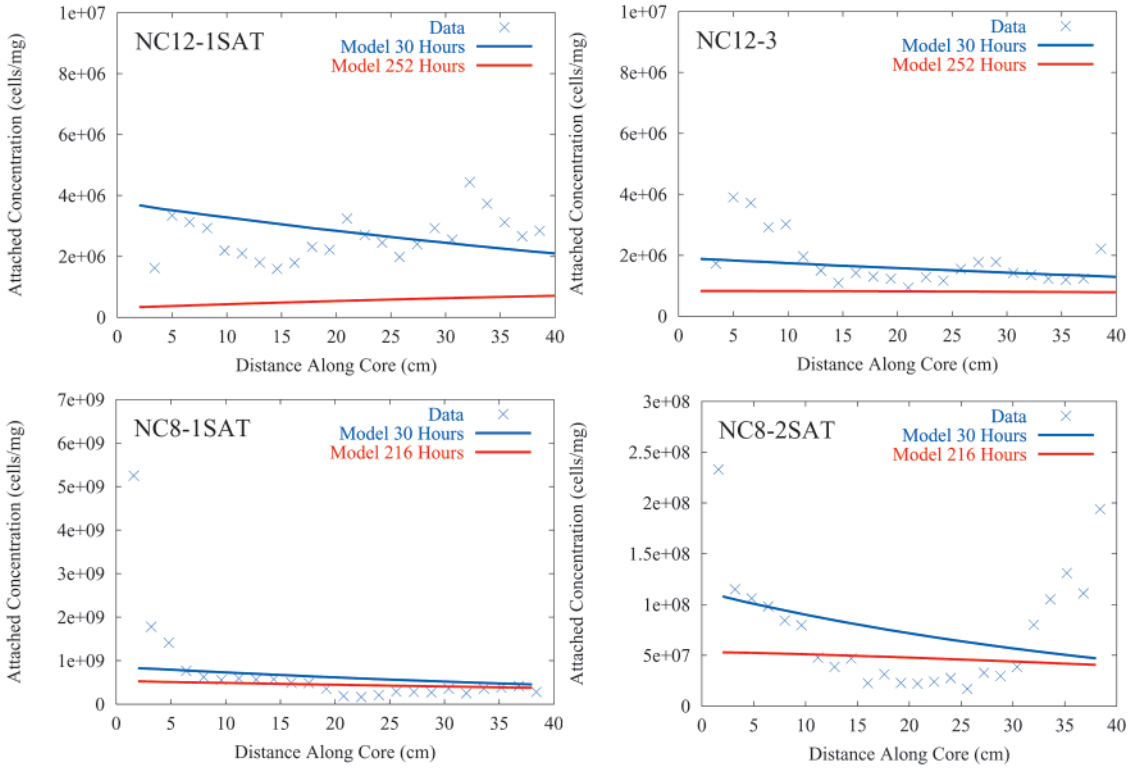

FIGURE 6. Observed and modeled bacterial attached profiles in the four cores: (a) NC12-1SAT, (b) NC12-3, (c) NC8-1SAT, and (d) NC8-2SAT. Model profiles are shown at 30 h and at the end of the experiments; observed profiles are at the end of the experiments when the cores were destructively subsampled.

responsible for the observed porosity reduction. The differential advection phenomenon is not present when the same bacteria are injected into a column of clean quartz of the similar grain size (*33*). When the same bacteria are injected into the NC field site, bacteria and Br breakthrough are nearly simultaneous (*15*). These results suggest that early breakthrough of the bacteria is unique to the cores, where the injected bacteria are forced to pass through a constrained column in the presence of the fine-grained, coating-rich bands.

Relative Dominance of Grain Size Over Metal Hydroxides. The enhanced bacterial retention on the bands of the metal hydroxides (Figure 2) may be illusive because it is actually caused by their small grain sizes and not their surface charges. Because the collision efficiency reflects the mutual interaction between bacterial and mineral surfaces, it can be argued that the correlation between α and the metal hydroxide may not be diagnostic of the mineralogical effect. This argument is valid if the injected bacteria are heterogeneous in their surface properties, thus making the sediment chemical effect difficult to isolate. Our data indicated that the injected bacterial population was relatively homogeneous. Assuming a constant surface potential of the sediment from NC8-1SAT, theoretical α can be predicted as a function of mobility of the injected cells (*18*). Conversely, theoretical α can be predicted as a function of sediment ζ-potential for a given bacterial mobility. The calculation is based on the extended DLVO theory (*34*), assuming a sphere-plate geometry and secondary minimum approach (*35*). The natural sediment is treated as a binary system with two components being DA001-quartz (Hamaker constant $= 4.1 \times 10^{-21}$ J) and DA001-organic carbon-coated iron/aluminum oxide (6.0×10^{-21} J) (18). If the average ζ-potential of the sediment is used (-5 mV), varying the mobility from -0.45 to -1.0 m^2 V^{-1} s^{-1} does not change α. If the mobility of the injected cells is kept constant (-0.45 m^2 V^{-1} s^{-1}), varying the ζ-potential from -3 to -6 mV changes α from 0.04 to 0.02. If the more negative mobility is used (-1.0 m^2 V^{-1} s^{-1}), varying the ζ-potential from -3 to -6 mV does not change α (0.02). If positive ζ-potential is used, resultant α becomes 1. These calculations indicate that the sediment is not sufficiently positive and heterogeneous to observe the chemical effect. If the sediment possesses a distribution of ζ-potential from positive to negative values, the collision efficiency will be correlated to such a range (i.e., from 1 to a small value), and the chemical effect will be operative. In this context, the studied bacteria−sediment is a model system for examining the physical effect.

Further evidence for the dominance of grain size comes from a comparison between the cores. The effluent recovery is approximately inversely correlated with grain size, independent of the abundance of the metal hydroxides (Table 2). The relative rate of the decrease of the retained bacterial concentration along the length of the cores is also correlated with grain size. For example, the steep decrease for NC8-1SAT is correlated with its small grain size, whereas the even distribution in NC12-1SAT is correlated with its relatively large grain size (Table 2).

In summary, the reasons for the lack of the chemical effects include a strain with a slightly negatively charged cell surface and the relatively uniform distribution of the metal hydroxides in the sediment. Although the cores displayed localized Fe and Al bands, these bands apparently did not show any significant positive surface charge because these bands possessed elevated adsorbed organic carbon (Figure 3b), resulting in the insignificant correlation between ζ-potential and the extractable Fe (Figure 3c). Organic matter has been shown to significantly reduce bacterial retention (*36*). The adsorbed organic matter concentration in the NC sediments falls between those for the uncontaminated and the contaminated sites in the Cape Cod aquifer (*37*) and appears typical in granular aquifers.

Attachment and Detachment. The higher core-scale values of K_f obtained from fitting breakthrough curve data

(relative to averages of the subcore grid estimates, Table 2) are required to account for the differential advection effect because of the kinetic nature of the attachment process as modeled. The enhanced velocity of bacteria leads to relatively shorter exposure times and therefore requires higher rate coefficients to represent the observed degree of attachment. Because the values of K_f estimated on the subcore grid are calculated using the velocity estimated from the Br data, they underestimate the actual attachment rate coefficients. The magnitude of the deviation between the two estimates increases as the differential advection factor increases (Table 2). When the values of K_f are recalculated using the velocity estimated from the bacterial data, the two estimates are closer, especially for core NC12-1SAT (data not shown).

The linear kinetic attachment and detachment model appears to be well-suited to represent the main pulse of bacterial breakthrough (Figure 4). We interpret the model's slight overestimation of bacterial breakthrough concentrations observed at longer times as reflecting partially irreversible attachment. This is also reflected in the slope of the modeled and observed attached bacteria profiles (Figure 6). At 30 h, shortly after the passage of the main pulse, the model predicts a decrease in attached concentration with distance from the influent end. Over longer periods of time, detachment and re-attachment causes a shift in the shape of the profile, and at the end of the experiment the model predicts increasing attached concentration with distance from the influent end. The data, however, display a generally flat slope, especially for cores NC12-1SAT and NC12-3, suggesting that some redistribution by detachment and re-attachment is occurring but not to the degree suggested by the fully reversible attachment model. This interpretation is supported by detailed modeling performed on similar core experiments by Wademan (*38*).

The increase in the attached concentrations near the effluent end observed in core NC8-2 is also contrary to model predictions. However, the core-scale model treats the core as one-dimensional and homogeneous with uniform attachment rate coefficient along the core length. Grain size and the abundance of the metal hydroxides, in contrast, vary with distance along the cores. In the case of core NC8-2, they exhibit a systematic trend with grain size decreasing and the metal hydroxide content increasing toward the effluent end. The attachment rate coefficients derived from the subcore grid reflect this trend, increasing toward the effluent end. Therefore, the deviation between the simulated, and observed profiles in this core may be attributed to subcore-scale variability in bacterial attachment rate coefficients.

Link of Laboratory to the Field. Mailloux et al. (*39*) successfully modeled the bacterial breakthrough in the field by using a distribution of collision efficiencies as determined from this study (as opposed to a single value), demonstrating value of laboratory core experiments. In other cases, however, model predictions based on uniform attachment rate coefficient derived from core experiments may underestimate the distance of bacterial movement in the field (*25*). This underestimation may be partly due to the time scale of desorption, where desorption may not be important in short-term core experiments but can be significant in the long-term transport in the field (*15*). Alternatively, the interaction of injected bacteria with groundwater and sediment under natural conditions may progressively alter their surface properties, creating heterogeneity in their surface properties.

This research demonstrates that bacterial retention in intact sediment cores is dominated by the physical attributes of the sediment (i.e., grain size) as opposed to the chemical properties (i.e., the metal hydroxide content) for the adhesion-deficient bacterial strain. The extended DLVO theory predicts α values that match the experimental α fairly well. The combination of the selected bacteria and the aquifer sediment provides a model system for understanding the physical control on bacterial transport. However, the experimental approach used in this study, when combined with the DLVO theory, provides guidance for future experiments where biological or chemical factors can be isolated and examined.

Acknowledgments

We acknowledge the support of the U.S. Department of Energy Natural and Accelerated Bioremediation Research Program (NABIR) (Grant DE-FG02-97ER62472). We also acknowledge the leadership of Dr. Frank Wobber, the Program Manager for the NABIR. We are indebted to The Nature Conservancy for access to the site for this project. We would like to thank Mr. Tim Griffin of Golder Associates for his excellent management of the field site operations. We would also like to thank Jessica Seebald, Lynne Elkins, and Doug Johnson for their assistance in conducting these experiments. Finally, we are grateful to five anonymous reviewers and the editor, Dr. Alexander Zehnder, for their efforts to significantly improve the early draft of the manuscript.

Literature Cited

(1) Harvey, R. W.; Garabedian, S. P. *Environ. Sci. Technol.* **1991**, *25*, 178−185.
(2) Steffan, R. J.; Sperry, K. L.; Walsh, M. T.; Vainberg, S.; Condee, C. W. *Environ. Sci. Technol.* **1999**, *33*, 2771−2781.
(3) Champ, D. R.; Schroeter, J. *Water Sci. Technol.* **1988**, *20*, 81−87.
(4) Jang, L.; Chang, P. W.; Findley, J. E.; Yen, T. F. *Appl. Environ. Microbiol.* **1983**, *46*, 1066−1072.
(5) Trevors, J. T., von Elsas, J. D.; van Overbeek, L. S.; Starodub, M. *Appl. Environ. Microbiol.* **1990**, *56*, 401−408.
(6) Updegraff, D. M. In *Modeling the Environmental Fate of Microorganisms*; Hurst, C. J., Ed.; American Society of Microbiology: Washington, DC, 1991.
(7) Macaskie, L. E.; Dean, A. C. R. *Biological Waste Treatment*; Alan R. Liss Inc.: New York, 1989.
(8) Olson, G. J.; Kelly, R. M. *Biotechnol. Proc.* **1988**, *2*.
(9) Hornberger, G. M.; Mills, A. L.; Herman, J. S. *Water Resour. Res.* **1992**, *28*, 915−923.
(10) DeFlaun, M. F.; Murray, C. J.; Holben, W.; Scheibe, T.; Mills, A.; Ginn, T.; Griffin, T.; Majer, E.; Wilson, J. L. *FEMS Microbiol. Rev.* **1997**, *20*, 473−487.
(11) Harvey, R. W.; Metge, D. W.; Kinner, N.; Mayberry, N. *Environ. Sci. Technol.* **1997**, *31*, 289−295.
(12) Ryan, J. N.; Elimelech, M. *Colloids Surf. A* **1996**, *107*, 1−56.
(13) Knapp, E. P.; Herman, J. S.; Hornberger, G. M.; Mills, A. L. *Environ. Geol.* **1998**, *33*, 243−248.
(14) Harvey, R. W. In *Manual of Environmental Microbiology*; Hurst, C. J., Knudsen, G. R., McInerney, M. J., Stetzenback, L. D., Walter, M. V., Eds.; ASM Press: Washington, DC, 1997.
(15) Johnson, W. P.; Zhang, P.; Fuller, M. E.; Scheibe, T. D.; Mailloux, B. J.; Onstott, T. C.; DeFlaun, M. F.; Hubbard, S. S.; Radtke, J.; Kovacik, W. P.; Holben, W. *Environ. Sci. Technol.* **2001**, *35*, 182−191.
(16) Fuller, M. E.; Streger, S. H.; Rothmel, R.; Mailloux, B. J.; Onstott, T. C.; Fredrickson, J. K.; Balkwill, D. L.; Deflaun, M. F. *Appl. Environ. Microbiol.* **2000**, *66*, 4486-4496.
(17) Fuller, M. E.; Dong, H.; Mailloux, B. J.; Onstott, T. C.; DeFlaun, M. F. *Water Resour. Res.* **2000**, 2417−2431.
(18) Dong, H.; Onstott, T. C.; Ko, C.-H.; Hollingsworth, A. D.; Brown, D. G.; Mailloux, B. J. *Colloids Surf. B* (in press).
(19) Dong, H.; Fredrickson, J. K.; Kennedy, D. W.; Zachara, J. M.; Kukkadapu, R. K.; Onstott, T. C. *Chem. Geol.* **2000**, *169*, 299−318.
(20) DeFlaun, M. F.; Oppenheimer, S. R.; Streger, S.; Condee, C. W.; Fletcher, M. *Appl. Environ. Microbiol.* **1999**, *65*, 759−765.
(21) DeFlaun, M. F.; Tanzer, A.; McAteer, A.; Marshall, B.; Levy, S. *Appl. Environ. Microbiol.* **1990**, *56*, 112−119.
(22) Dong, H.; Onstott, T. C.; DeFlaun, M. F.; Gillespie, K.; Fedrickson, J. K. *J. Microbiol. Methods* **1999**, 139−154.
(23) Sverjensky, D. A.; Sahai, N. *Geochim. Cosmochim. Acta* **1996**, *60*, 3773−3797.
(24) Jackson, M. L.; Lim, C. H.; Zelanzy, L. W. In *Methods of Soil Analysis, Part 1. Physical and Mineralogical Methods*, 2nd ed.; American Society of Agronomy−Soil Science Society of America: Madison, WI, 1986.

(25) Scheibe, T. D.; Chien, Y.-J.; Radtke, J. S. *Ground Water* **2001**, *39*, 210−222.
(26) Toride, N.; Leij, F. J.; van Genuchten, M. Th. *The CXTFIT code for estimating transport parameters from laboratory or field tracer experiments, Version 2.1*; U.S. Salinity Laboratory, Agricultural Research Service, U.S. Department of Agriculture: Washington, DC, 1995.
(27) Logan, B. E.; Jewett, D. G.; Arnold, R. G.; Bouwer, E. J.; O'Melia, C. R. *J. Environ. Eng.* **1995**, 869−872.
(28) Bales, R. C.; Gerba, C. P.; Grondin, G. H.; Jensen, S. L. *Appl. Environ. Microbiol.* **1989**, *55*, 2061−2067.
(29) Toran, L.; Palumbo, A. V. *J. Contam. Hydrol.* **1992**, *9*, 289−303.
(30) Powelson, D. K.; Gerba, C. P.; Yahya, M. T. *Water Res.* **1993**, *27*, 583−590.
(31) Ginn, T. R. *Water Resour. Res.* **2000**, *36*, 1981−1982.
(32) Rehmann, L. L. C.; Welty, C.; Harvey, R. W. *Water Resour. Res.* **2000**, *36*, 1983−1984.
(33) Long, K. L. Princeton University, 2000.
(34) Grasso, D.; Smets, B. F.; Srevett, D. A.; Machinist, B. D.; vas Oss, C. J.; Glese, R. F. *Environ. Sci. Technol.* **1996**, *30*, 3604−3608.
(35) Simoni, S. S.; Harms, H.; Bosma, T. N. P.; Zehnder, A. J. B. *Environ. Sci. Technol.* **1998**, *32*, 2100−2105.
(36) Johnson, W. P.; Logan, B. E. *Water Res.* **1996**, *30*, 923−931.
(37) Scholl, M. A.; Harvey, R. W. *Environ. Sci. Technol.* **1992**, *26*, 1410−1417.
(38) Wademan, M. C. Master of Science Thesis, University of California, Davis, 2000.
(39) Mailloux, B. J.; Onstott, T. C.; Hall, J.; Fuller, M. E.; DeFlaun, D. F.; Dong, H. *AGU Fall Meet.* **2000**, *81*, F181.

Received for review May 28, 2001. Revised manuscript received October 17, 2001. Accepted December 5, 2001.

ES010144T